International Journal of Engineering Science 193 (2023) 103943

Contents lists available at ScienceDirect

International Journal of Engineering Science

journal homepage: www.elsevier.com/locate/ijengsci

Reduced order modeling of parametrized pulsatile blood flows: Hematocrit percentage and heart rate

Catalina Farías [a], Camilo Bayona-Roa [b], Ernesto Castillo [a,*], Roberto C. Cabrales [c], Ricardo Reyes [d]

[a] *Departamento de Ingeniería Mecánica, Universidad de Santiago de Chile, Avenida Libertador Bernardo O Higgins 3363, Santiago, Chile*
[b] *Departamento de Ingeniería Industrial, Facultad de Ingeniería, Pontificia Universidad Javeriana, Bogotá, Colombia*
[c] *Instituto Multidisciplinario de Investigación y Postgrado, Universidad de La Serena, Avenida Raúl Bitrán 1305, La Serena, Chile*
[d] *Chair of Computational Mathematics and Simulation Science, École Polytechnique Fédérale de Lausanne, EPFL, 1015, Lausanne, Switzerland*

ARTICLE INFO

Keywords:
Hemodynamics
Reduced-order-modeling
Parametrized Solutions
Variational Multiscale Method
Blood Rheology

ABSTRACT

This paper numerically evaluates the accuracy and performance of a stabilized finite element Reduced Order Modelling (ROM) approach that is designed to simulate pulsatile blood flows. The method is able to estimate fluid flow parametric solutions of interest in hemodynamics by considering the hematocrit percentage (Hct%) and the heart rate (f_c) as parameters. The method estimates off-trained parametric scenarios which have not been included in the training data set composing the ROM basis and that can adopt arbitrary values from specific patient conditions. The hematocrit percentages modifies the viscous properties of blood, which are incorporated into the problem physics through a power-law model. The hematocrit percentages are $5 \leq$ Hct% ≤ 50, ranging from severe anemia to physiological values. The pulsatile flow condition is modeled via a Womersley function, with $f_c$bpm (beats per minute) ranging between 60bpm $\leq f_c \leq$ 120bpm. These frequencies comprise physiological conditions of patients at rest and tachycardia or moderate exercise. Two-and-three-dimensional flows are simulated inside a representative geometry of a carotid artery, where the accuracy is tested by studying the effect of the number of components of the ROM approximating basis and the number of sampling points composing the training data set. The parametric calculation verifies that the proposed approach constitutes a valuable computational tool for simulating complex fluid flow hemodynamics and can be applied to clinical decision-making.

1. Introduction

Atherosclerotic cardiovascular disease is one of the most important cardiovascular diseases in the world (Libby et al., 2019), with low- and middle-income countries accounting for at least 80% of cases (de Mestral & Stringhini, 2017; Schultz et al., 2018). Atherosclerosis is when lipids build up in the inner walls of the arteries in the form of atherosclerotic plaque (Badimon & Vilahur, 2014; Seidman, Mitchell, & Stone, 2014). That disease occurs in vascular regions where flow shear-stresses are low, and separation or re-circulation patterns appear (Blake, Meagher, Fraser, Easson, & Hoskins, 2008; Davies, 2009; Irace et al., 2012; Malek, Alper, & Izumo, 1999). Computational Fluid Dynamics (CFD) has proven valuable and reliable in visualizing/understanding blood circulation. CFD allows a detailed description of vascular flow, formerly unavailable due to impracticable *in-vivo* measurements (Debbich et al.,

* Corresponding author.
E-mail address: ernesto.castillode@usach.cl (E. Castillo).

https://doi.org/10.1016/j.ijengsci.2023.103943
Received 30 January 2023; Received in revised form 11 August 2023; Accepted 12 August 2023
Available online 25 August 2023

2020; Schussnig, Pacheco, Kaltenbacher, & Fries, 2022; Steinman & Taylor, 2005; Xu et al., 2018). Thus, supporting non-invasive diagnoses and image-based medical examinations (Coenen et al., 2018; Taylor, Fonte, & Min, 2013).

Blood is a non-homogeneous non-linear complex fluid composed of red blood cells, white blood cells, and platelets suspended in a Newtonian fluid called plasma (Agarwal, Katiyar, & Pradhan, 2008; Ayyaswamy, 2016). Plasma is mainly composed of water but also contains several proteins dissolved and a variety of ions, including sodium, calcium, magnesium, and potassium (see Anand & Rajagopal, 2004, 2017; Anand, Rajagopal, & Rajagopal, 2003, 2006 for an exhaustive detail). Blood can be modeled using a suitable combination of continuum mechanics and experimental data, giving place to Non-Newtonian constitutive models. Overall, blood behaves as a non-Newtonian fluid that depends on the hematocrit percentage (Ameenuddin, Anand, & Massoudi, 2019; Nader et al., 2019; Steinman, 2012), which indicates the number of red blood cells. The rheological relation between forces and fluid deformations depends on the vascular geometry and blood composition. For example, blood behaves as a Newtonian fluid in large arteries with high shear-stresses ratios (Sequeira & Janela, 2007). Low shear-stress zones are present in curved arteries with bifurcations or stenosis making blood behave as a non-Newtonian fluid (Chauhan & Sasmal, 2021; Misra & Shit, 2006; Yilmaz & Gundogdu, 2008). Non-Newtonian blood rheology could be very complex, as reported in Anand and Rajagopal (2004, 2017), Huang et al. (1975) and Thurston (1973) where shear-thinning and viscoelastic behaviors have been reported and discussed. From experimental macro-rheology studies, blood can be defined as a purely viscous fluid with a predominant shear-thinning behavior as Charm and Kurland (1965) and Chien, Usami, Taylor, Lundberg, and Gregersen (1966). In this sense, shear-thinning models can be described using the power-law model (Abugattas, Aguirre, Castillo, & Cruchaga, 2020; Mandal, 2005; Mendieta et al., 2020), the Carreau model (Lee & Steinman, 2007; Mendieta et al., 2020; Morbiducci et al., 2011), the Carreau-Yasuda model (Box, Van Der Geest, Rutten, & Reiber, 2005; Gharahi, Zambrano, Zhu, DeMarco, & Baek, 2016), the Cross model (Abugattas et al., 2020; Mendieta et al., 2020), and the Casson model (Suzuki et al., 2021).

Macro-circulation refers to the blood flow in large vessels. The flow pattern in those vessels depends primarily on the hematocrit level (Baskurt & Meiselman, 2003) and plasma protein concentration (Walburn & Schneck, 1976). However, the effect on viscosity due to plasma protein variation is less significant than the hematocrit variation (Guyton & Hall, 2006). In this context, most rheological models employ the physiologic 40 to 45% hematocrit range (Robertson, Sequeira, & Kameneva, 2008). The hematocrit level may vary between patients depending on gender, age, pregnancy, or anemia. For non-pregnant adult women, hematocrit varies in the 37% to 47% range, while for adult men, this value shifts from 40% to 54%. Hematocrit may drop to 10% for anemic patients, while it may range between 60% and 70% in polycythemia (Guyton & Hall, 2006; Robertson et al., 2008). Some unified models aim to describe the blood flow covering a wide range of hematocrit values. In this context, the Walburn & Schneck model (Walburn & Schneck, 1976), whose formulation directly relates the shear-thinning behavior of blood and the patient's hematocrit and protein concentration, is a classical reference. In Lee and Steinman (2007), a Newtonian viscosity model depending on the hematocrit percentage was proposed. More recently, in Ameenuddin et al. (2019) a model which incorporates hematocrit variations in the shear-thinning Yeleswarapu viscosity relation was presented showing good qualitative agreement with other studies.

Blood flow is pulsatile and, therefore, transient by definition. A common simplification in the context of hemodynamics is to consider it stationary, which in large arteries such as the carotid artery is physically incorrect. The flow dynamics are dependent on the influence of the heart rate and vascular wall tensions. The pulsatile behavior in CFD models is reconstructed from Doppler, MRI fluxes (Debbich et al., 2020) or through empirical mathematical functions such as the one proposed by Womersley in Womersley (1955). That model allows the space and time definition of the blood flux or velocity depending on the heart pulse rate. Womersley's model has been recurrently used in the context of CFD, with satisfactory and representative outcomes in blood flow dynamics (Cebral, Castro, Soto, Löhner, & Alperin, 2003; Taylor, Hughes, & Zarins, 1998; Wei et al., 2019; Xu et al., 2018).

Full-Order Methods (FOM) applied to the fluid dynamics simulation have proven valuable and reliable in hemodynamics. FOM techniques, such as the Finite Element Method (FEM) or the Finite Volume Method (FVM) (to name a few), require high computational costs and long calculation times when solving time-dependent flows (Lassila, Manzoni, Quarteroni, & Rozza, 2014; Li et al., 2021). The study of specific-patient problems requires the input of physical properties, boundary conditions, and geometries, which vary by individual. Different hemodynamic models have been developed to reduce calculation times and optimize flow simulations. For example, the statistical approaches in Benner, Gugercin, and Willcox (2015) and Eldred and Dunlavy (2006) are directly related to the application of machine learning both in hemodynamics (Gao, Zhu, & Wang, 2020; Li et al., 2021; Sankaran, Grady, & Taylor, 2015) and in cardiovascular biomechanics (Buoso, Joyce, & Kozerke, 2021). Also, ROM has been developed to address variability of cardiovascular geometries (Ballarin et al., 2016; Galarce, Lombardi, & Mula, 2022; Manzoni, Quarteroni, & Rozza, 2012), where flow dynamics are responses of topological characteristics. In Siena, Girfoglio, Ballarin, and Rozza (2023), the use of a machine learning-based reduced order model to address physical and geometrical variations related to the inlet flow condition and the stenosis severity in a coronary artery was analyzed using the finite volume method.

In this work, the VMS-ROM formulation proposed in Reyes, Ruz, Bayona-Roa, Castillo, and Tello (2023), which allows for solving time-dependent flows of power-law fluids, is applied to analyze a pulsatile blood flow in a two and three-dimensional carotid artery. The shear-thinning rheological behavior of blood is incorporated in the numerical experiments using the Walburn & Schneck model (Walburn & Schneck, 1976) for a hematocrit percentage ranging between $35\% < \mathrm{Hct}\% < 50\%$. Also, a severe anemia condition is analyzed for hematocrits of 5%, 10%, and 15%, using the viscosity parameters proposed in Mehri, Mavriplis, and Fenech (2018). The use of these references is based on the years of existence of the Walburn & Schneck model and the broad spectrum of hematocrits covered by the other references, however, any other purely viscous model could be considered in our numerical framework. The Womersley profile characterizes frequency rates from 60 to 120 beats per minute (bpm). The reduced order approximations include the composition of bases of more than one physical problem and flow condition, including variations in the hematocrit percentage and frequency rates. We employ a simplified Tucker decomposition that uses the Singular Value

Table 1
List of m and n values for the Hct percentages.

Hct%	5	10	15	35	40	45	50
m	0.0093	0.0108	0.0171	0.0089	0.0115	0.0148	0.0191
n	0.6600	0.6800	0.5680	0.8254	0.8004	0.7754	0.7505

Decomposition (SVD) over a flattened or unfolded data set of high rank. The combination of these techniques allows us to simulate off-trained parametric scenarios which have not been included in the training data set, being the arbitrary scenario of patient-specific conditions the main goal to pursue. To our knowledge, this has not been reported.

The article content is as follows. Section 2 recalls the models and governing equations that describe the pulsatile blood flow. Section 3 introduces the physical problem and the carotid artery geometries. In Section 4, the results obtained for the two-dimensional case are presented, including a sensitivity study of the mesh and the time step size used in the ROM simulations. Section 5 includes the three-dimensional extension of the ROM technique. Finally, the conclusions and some remarks of the work are in Section 6.

2. Governing equations and models

2.1. The Navier–Stokes equations

We consider the time-dependent Navier–Stokes equations for a power-law fluid on a finite time interval $t \subset \left]0, t_f\right[$ and in an open, connected, bounded Lipschitz domain $\Omega \subset \mathbb{R}^d$ with dimension $d = 2$ or 3, and boundary $\partial\Omega$. The isothermal fluid flow problem is given by

$$\rho\frac{\partial \boldsymbol{u}}{\partial t} + \rho\boldsymbol{u}\cdot\nabla\boldsymbol{u} - \nabla\cdot(2\eta(\boldsymbol{u})\nabla^s\boldsymbol{u}) + \nabla p = \boldsymbol{f}, \qquad \text{in } \Omega,\ t \in \left]0, t_f\right[, \tag{1}$$

$$\nabla\cdot\boldsymbol{u} = 0, \qquad \text{in } \Omega,\ t \in \left]0, t_f\right[. \tag{2}$$

The velocity vector field and pressure are the problem unknowns, being $\boldsymbol{u}$ and p, respectively. The fluid properties are the density ρ and the apparent viscosity $\eta(\boldsymbol{u})$ defined by the power-law model. The right-hand side body force vector is represented by $\boldsymbol{f}$. Note that bold characters refer to vectors and tensors.

This scosity models, including the percentage of hematocrit obtained in Mehri et al. (2018) and Walburn and Schneck (1976) through experimental analysis. Both models adjusted the parameters using the power-law model, which is defined as:

$$\eta(\boldsymbol{u}) = m\dot{\gamma}^{n-1}, \tag{3}$$

where $\dot{\gamma} = \sqrt{\frac{1}{2}(\dot{\boldsymbol{\gamma}} : \dot{\boldsymbol{\gamma}})}$ represents a magnitude of the rate of deformation tensor $\dot{\boldsymbol{\gamma}} = \nabla\boldsymbol{u} + (\nabla\boldsymbol{u})^T$. The constitutive parameters are the consistency index m and the power-law index n. Both indices depend on the hematocrit amount and are defined using the Walburn-Schenck model (Walburn & Schneck, 1976) through the following expressions

$$m = C_1 e^{C_2(\mathrm{Hct})}, \qquad n = 1.0 - C_3(\mathrm{Hct}), \tag{4}$$

where $C_1 = 0.00148\ \mathrm{Pa\,s}^n$, $C_2 = 0.0512$, and $C_3 = 0.00499$ are model parameters and Hct represents the hematocrit value ranging between 35% and 50%. To represent hematocrits lesser than 35%, the values proposed in Mehri et al. (2018) for hematocrits of 5, 10, and 15% are used. As notation, the different percentages of hematocrit are defined with the letter H followed by the number associated with the percentage of hematocrit. So H45 represents a hematocrit of 45%. Overall power-law and consistency indexes used in this work are included in Table 1.

Additionally, a Newtonian viscosity of $\mu = 0.00345\,\mathrm{Pa\,s}$ is used in some calculations to compare the effect of hematocrit and evaluate the shear-thinning behavior of blood. A fixed density value of $\rho = 1050\ \mathrm{kg/m^3}$ is used for all cases (Abugattas et al., 2020).

2.2. Pulsatile boundary condition

The Womersley profile defines a periodic pulsatile flow widely used for blood flow (Blake et al., 2008; Cebral et al., 2003; Taylor et al., 1998). The Womersley equation defines the inlet component of velocity as a function of the azimuthal radius, r, and time, t. The radius of the artery is denoted by R. Following the proposed in Blake et al. (2008), the pulsatile inlet boundary condition can be defined as

$$v(r,t) = 2V_0\left[1 - \left(\frac{r}{R}\right)^2\right] + \sum_{l=1}^{N}\Re\left\{V_l e^{i(l\omega t - \psi_l)}\left[\frac{J_0\left(\beta_l\right) - J_0\left(\beta_l\frac{r}{R}\right)}{J_0\left(\beta_l\right) - 2J_1\left(\beta_l\right)/\beta_l}\right]\right\}, \tag{5}$$

where $l = 1, \ldots, N$ is the lth harmonic, $\Re\{.\}$ represents the real part of a complex function with i the imaginary unit, V_l represents the Fourier components for the mean velocity, ψ_l represents the phase, and J_0 and J_1 are the Bessel functions of the first kind of order 0 and 1, respectively. Also, ω represents the heart rate in (rad/s). The parameter β_l is obtained from the expression

$$\beta_l = W_{o,l}\, i^{3/2}, \tag{6}$$

Table 2
Fourier components and phase values for the first eleven harmonics.

l	0	1	2	3	4	5	6	7	8	9	10
V_l	0.2625	0.0885	0.0892	0.0666	0.0517	0.0470	0.0268	0.0119	0.0072	0.0040	0.0017
ψ_l	0	0.802	1.261	1.956	2.288	2.94	−2.583	−2.286	−2.131	−1.926	−1.368

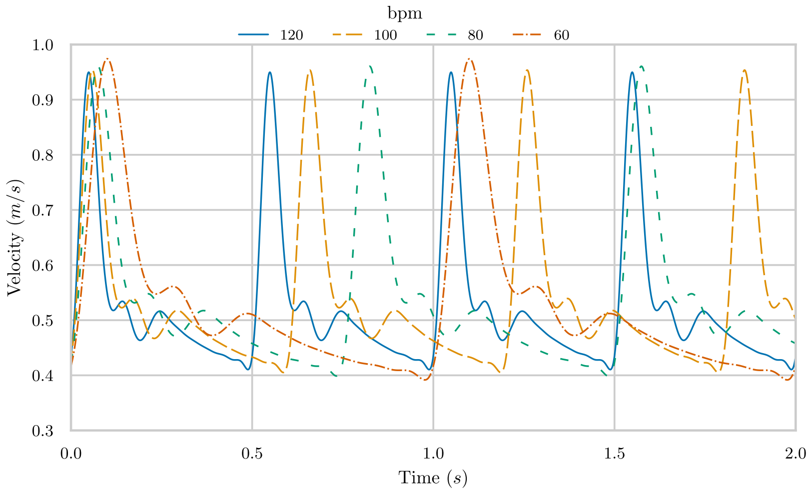

Fig. 1. Inlet velocity evolution at $r = 0$ as a function of the heart rates.

where $W_{o,l}$ represents the Womersley number for each harmonic, defined as

$$W_{o,l} = R\sqrt{\frac{\rho l \omega}{\mu}}. \tag{7}$$

When $l = 1$, we just write W_o.

The profile parameters in this study have been obtained from Piskin and Serdar Celebi (2013) after applying the fast Fourier transform. The maximum and average velocity of the cardiac cycle ensures the blood flux in a typical carotid artery (Holdsworth, Norley, Fraynek, Steinman, & Rutt, 1999). The amplitude and phase values are listed in Table 2.

In this work, the blood flow is considered inside the $f_c = 60$ bpm (1.333 Hz) to $f_c = 120$ bpm (2.0 Hz) heart rate range, corresponding to $5.5 \leq W_o \leq 7.8$. Note that 60 bpm $\leq f_c \leq$ 100 bpm is considered normal for resting states (Spodick, 1992) and $f_c = 120$ bpm can be associated with tachycardia or moderate exercise. The Womersley profile considers a constant viscosity $\nu = \mu/\rho$. Fig. 1 shows the inlet velocity evolution in the middle of the artery as a function of the different heart rates.

2.3. Stabilized finite element method

Our interest in the present study is the simulation of dominant convective blood flows. Therefore, a stabilized finite element formulation is used. That formulation also allows equal order interpolation between velocity and pressure fields. The stabilized formulation was proposed in Castillo and Codina (2019) and has been numerically tested in the context of incompressible Newtonian and non-Newtonian fluids in González, Cabrales, and Castillo (2022), González, Castillo, and Cruchaga (2020) and Osses, Castillo, and Moraga (2021). The distinctive features of this formulation are its non-residual structure, which is unusual in the context of stabilized formulations, and its dynamic nature, which is associated with incorporating time derivatives in the subscale equations.

Let us introduce some standard notation. The space of square-integrable functions in the domain Ω is denoted by $L^2(\Omega)$, and the space of functions whose distributional derivatives of order up to $m \geq 0$ (integers) that belong to $L^2(\Omega)$ is $H^m(\Omega)$. The space $H_0^1(\Omega)$ consists of functions in $H^1(\Omega)$ that vanish at the boundary $\partial\Omega$. The topological dual of $H_0^1(\Omega)$ is denoted by $H^{-1}(\Omega)$, the dual pairing between two functions by $\langle\cdot,\cdot\rangle$, and the L^2–inner product in Ω, for scalar, vectors, and tensors is denoted by $(\cdot,\cdot)$. Based on the above, we define $\mathcal{V} = \left(H_0^1(\Omega)\right)^d$ and $\mathcal{Q} = L^2(\Omega)/\mathbb{R}$ as the spaces of $\boldsymbol{u}$ and p, respectively. Denoting $\boldsymbol{\mathcal{X}} := \mathcal{V} \times \mathcal{Q}$, and using conforming finite element spaces, such that $\mathcal{V}_h \subset \mathcal{V}$, $\mathcal{Q}_h \subset \mathcal{Q}$, and $\boldsymbol{\mathcal{X}}_h := \mathcal{V}_h \times \mathcal{Q}_h$, the stabilized finite element method consists in finding $\boldsymbol{U}_h = [\boldsymbol{u}_h, p_h] : \,]0, t_f[\, \to \boldsymbol{\mathcal{X}}_h$, such that

$$\begin{aligned} \rho\left(\frac{\partial \boldsymbol{u}_h}{\partial t}, \boldsymbol{v}_h\right) + B\left(\hat{\boldsymbol{u}}_h; \boldsymbol{U}_h, \boldsymbol{V}_h\right) + \sum_K \tau_2\left(\hat{\boldsymbol{u}}_h\right)\left(\nabla\cdot\boldsymbol{v}_h, P_h^{\perp}\left(\nabla\cdot\boldsymbol{u}_h\right)\right)_K \\ - \sum_K \left(\rho\hat{\boldsymbol{u}}_h\cdot\nabla\boldsymbol{v}_h, \tilde{\boldsymbol{u}}_1\right)_K - \sum_K \left(\nabla q_h, \tilde{\boldsymbol{u}}_2\right)_K = \langle \boldsymbol{f}, \boldsymbol{v}_h\rangle, \end{aligned} \tag{8}$$

where

$$B\left(\hat{\boldsymbol{u}}_h;\boldsymbol{U}_h,\boldsymbol{V}_h\right)=\left(2\eta(\hat{\boldsymbol{u}}_h)\nabla^s\boldsymbol{u}_h,\nabla^s\boldsymbol{v}_h\right)+\langle\rho\hat{\boldsymbol{u}}_h\cdot\nabla\boldsymbol{u}_h,\boldsymbol{v}_h\rangle-\left(p_h,\nabla\cdot\boldsymbol{v}_h\right)+\left(\nabla\cdot\boldsymbol{u}_h,q_h\right)$$

for all $\left[\boldsymbol{v}_h,q_h\right]\in\mathcal{X}_h$, where $\boldsymbol{f}\in H^{-1}(\Omega)$ is assumed. The velocity subscales $\tilde{\boldsymbol{u}}_1$ and $\tilde{\boldsymbol{u}}_2$ come from the resolution of

$$\rho\frac{\partial\tilde{\boldsymbol{u}}_1}{\partial t}+\tau_1^{-1}\left(\hat{\boldsymbol{u}}_h\right)\tilde{\boldsymbol{u}}_1=-P_h^{\perp}\left(\rho\hat{\boldsymbol{u}}_h\cdot\nabla\boldsymbol{u}_h\right),\tag{9}$$

$$\rho\frac{\partial\tilde{\boldsymbol{u}}_2}{\partial t}+\tau_1^{-1}\left(\hat{\boldsymbol{u}}_h\right)\tilde{\boldsymbol{u}}_2=-P_h^{\perp}\left(\nabla p_h\right).\tag{10}$$

The stabilization parameters $\tau_1\left(\hat{\boldsymbol{u}}_h\right)$ and $\tau_2\left(\hat{\boldsymbol{u}}_h\right)$, are defined by

$$\tau_1\left(\hat{\boldsymbol{u}}_h\right)=\left(\rho\frac{c_1\eta(\hat{\boldsymbol{u}}_h)}{\left(h_1\right)^2}+\rho\frac{c_2|\hat{\boldsymbol{u}}_h|}{h_2}\right)^{-1},\qquad\tau_2\left(\hat{\boldsymbol{u}}_h\right)=\frac{\left(\frac{h_1}{k^2}\right)^2}{c_1\tau_1\left(\hat{\boldsymbol{u}}_h\right)},\tag{11}$$

where h_1 and h_2 represents two characteristic element lengths. The characteristic length h_1 is computed as the square root of the element area for the 2D case and as the cube root for 3D problems. Characteristic length h_2 represents the element length in the streamline direction. Algorithmic parameters $c_1=2$ and $c_2=4$ are used in this work in all the calculations. We refer to Buscaglia, Basombrío, and Codina (2000) and Codina (1998) for a study of the effect of these parameters. The rheological behavior of the fluid is through the apparent viscosity in the definition of the stabilization parameters.

In this work, the nonlinear problem is solved iteratively, considering that:

- The convective term of the momentum equation, the apparent viscosity, and the stabilization parameters $\tau_1\left(\hat{\boldsymbol{u}}_h\right)$ and $\tau_2\left(\hat{\boldsymbol{u}}_h\right)$ are linearized using Picard's method.
- The orthogonal projection, for any function f, is iteratively approximated within the non-linearity loop of the problem, so that $P_h^{\perp}\left(f^i\right)\approx f^i-P_h\left(f^{i-1}\right)$.

The second order backward differentiation scheme is used for the time derivative of the linear momentum equation, which is defined as

$$\left.\frac{\partial\boldsymbol{u}_h}{\partial t}\right|_{t^{j+1}}=\frac{3\boldsymbol{u}_h^{j+1}-4\boldsymbol{u}_h^{j}+\boldsymbol{u}_h^{j-1}}{2\delta t}+\mathcal{O}\left(\delta t^2\right),\tag{12}$$

where $\delta t=t_f/N_t$ is the size of a uniform partition of the time interval $]0,t_f[$, and $\mathcal{O}(\cdot)$ is the order of approximation of the scheme. The superscript indicates the time step at which the variable is being approximated, such that $\boldsymbol{u}^j$ is an approximation of $\boldsymbol{u}$ at time $t^j=j\delta t$ for $j=0,\dots,N_t$.

The dynamic formulation of the VMS method is obtained by discretizing in time the equations of the sub-scales (9) and (10) through a first-order backward integration scheme, which does not affect the optimal convergence order of the method (Castillo & Codina, 2019; Codina, Principe, Guasch, & Badia, 2007).

2.4. Parametric reduced order model

The reduced model in this paper allows the solution of multiple parameters of the problem. For instance, the time t at transient solutions or the fluid rheology parameters. That is possible through the appropriate construction of the reduced approximation of the unknowns. Let $\mathsf{P}=\{\mathsf{P}_1,\dots,\mathsf{P}_{n_{par}}\}$ be a set of vectors comprising the Hematocrit and Heart Rate parameters of the problem (in example, $\mathsf{P}_1=[\mathrm{Hct}_1,\mathrm{bpm}_1]^T$). For each $\mathsf{P}_m\in\mathsf{P}$ problem, one can write the corresponding Finite Element approximation of the unknowns in $\boldsymbol{\mathcal{X}}_h=\mathrm{span}\{\boldsymbol{\varphi}^a_{\mathrm{FOM}}(\boldsymbol{x})\ :\ a=1,\dots,n_{dof}\}$ as

$$\boldsymbol{U}_h(\boldsymbol{x},t;\mathsf{P}_m):=\sum_{a=1}^{n_{dof}}\boldsymbol{\varphi}^a_{\mathrm{FOM}}(\boldsymbol{x})U^a_{\mathrm{FOM}}(t;\mathsf{P}_m),\tag{13}$$

where $U^a_{\mathrm{FOM}}(t;\mathsf{P}_m)\in\mathbb{R}$ are the $n_{dof}-$spatial unknowns of the problem at each time instant t. Solving problem (8) with (13) is commonly known as Full Order Model (FOM).

The *off-line* part of the proposed method comprises the construction of the reduced basis approximation through statistical techniques over physical FOM solutions of the problem. For each $\mathsf{P}_m\in\mathsf{P}$, and a given collection of selected time instants $\mathsf{T}=\{\mathsf{t}^1,\dots,\mathsf{t}^{n_s}\}$, the set of collected *snapshots* is defined by

$$\boldsymbol{\mathcal{S}}_m=\{\boldsymbol{U}_h(\boldsymbol{x},\mathsf{t}^1;\mathsf{P}_m),\dots,\boldsymbol{U}_h(\boldsymbol{x},\mathsf{t}^{n_s};\mathsf{P}_m)\}\subset\boldsymbol{\mathcal{X}}_h.\tag{14}$$

For $j=1,\dots,n_s$, we denote by U^j_m, the vector of $\mathbb{R}^{n_{dof}}$ with components $\mathsf{U}^j_{m,a}=U^a_{\mathrm{FOM}}(t^j;\mathsf{P}_m)$, $a=1,\dots,n_{dof}$. Thus, $\mathsf{U}^j_{m,a}$, store the coefficients of the FOM solution for each computational node $\boldsymbol{x}_a$ at time level t^j calculated for each problem with parameters in P_m. By using these vectors, we construct the high-rank matrix $\mathbf{U}=\left[\mathsf{U}^j_{ma}\right]\in\mathbb{R}^{n_{dof}\times n_s\times n_{par}}$ with n_{dof} rows, n_s columns, and n_{par} deep. This is a matrix of n_{par} pages with each one being of order $n_{dof}\times n_s$ as depicted in Fig. 2(a). For $m=1,\dots,n_{par}$, we denote by $\mathbf{U}^{(m)}\in\mathbb{R}^{n_{dof}\times n_s}$ the mth page of the $\mathbf{U}$ matrix.

We employ a partial Tucker decomposition as the one used in Reyes et al. (2023), which aims to decompose the matrix $\mathbf{U}$ into a set of rank-two matrices and one small core tensor. The classic strategy is followed, where the flattening of $\mathbf{U}$ is performed solely for